Interfacial transport in porous media: Application to dc electrical conductivity of mortars

Lawrence M. Schwartz,[a] Edward J. Garboczi, and Dale P. Bentz
National Institute of Standards and Technology, Building Materials Division, 226/B350, Gaithersburg, Maryland 20899

(Received 10 May 1995; accepted for publication 9 August 1995)

A mortar is a composite of inert sand grains surrounded by a porous cement paste matrix. We investigate the electrical conductivity of model mortars that include enhanced electrical conduction in the matrix–sand grain interfacial region. The electrical conductivity is evaluated by a combination of finite element, finite difference, and random walk methods for periodic and disordered models of mortar. Since the effective conductivity within the interfacial zone is often much higher than the bulk matrix conductivity, the qualitative features of transport in these systems is often controlled by the connectivity of the interfacial zone. Special attention is thus given to the geometrical percolation of this zone. A family of effective medium approximations give a good qualitative description of the disordered model's electrical properties. A simple four parameter Padé approximant is found to successfully describe the electrical conductivity of the periodic model over the entire range of parameters studied. Finally, we show that our calculations can be used to obtain a reasonable estimate of the permeability to viscous fluid flow. © *1995 American Institute of Physics.*

I. INTRODUCTION

The transport properties of porous media are of interest in connection with a variety of environmental, infrastructural, and technological problems. Among the systems of interest are heterogeneous catalysts, reservoir rocks, and cement-based materials like mortar and concrete. Concrete is a generic term describing a mixture of cement paste and inert aggregate particles usually comprised of sand grains and rock fragments. (Cement paste is, itself, a porous material formed by the hydration of cement powder.) In a mortar, the aggregate particles are limited to sand grains whose diameter typically does not exceed a few millimeters.

The dc electrical conductivity of mortar and concrete is important both as a means of probing the structure of these materials and as a measure of ionic diffusivity,[1] via the Nernst–Einstein relation.[2] Diffusivity is of interest in connection with a range of issues related to durability; examples are sulfate attack and chloride ion-induced corrosion of steel reinforcing bars.[3] These materials conduct electricity via the electrolytic pore fluid[4–6] in the cement paste matrix. The conductivity of paste depends on the original water-cement mixing ratio, the cement chemistry, the curing conditions, and the curing time. At a given time, however, the paste may be viewed as a composite of water, unhydrated cement powder, and the various chemical reaction products. Much recent work has been done on understanding how the complex microstructure of cement paste determines its electrical conductivity.[4–7] However, relatively little work has been done on how the conductivity of concrete depends on quantities like the density and size distribution of aggregate particles and on the geometry and properties of the cement paste-aggregate interfacial zone.[6]

This paper is concerned with the influence (on the transport properties of the mortar composite) of the interfacial zone that separates the aggregate grains from the bulk cement paste. We emphasize that interfacial effects are important in a variety of different physical systems. One particularly striking example involves random mixtures of ionic conductors and ionic insulators.[8–10] Another example, closer to the systems studied here, involves electrochemical effects in clay rich reservoir rocks.[11] In both these systems, as in the mortars of interest here, the presence of the interface can lead to enhanced electrical conduction. Thus, while all three materials might naively be viewed as *two* phase composites, a proper description of their transport properties requires a *three* phase analysis in which the interface is treated on an equal footing with the other two components.

II. THREE PHASE (HARD CORE-SOFT SHELL) MODEL

A. General remarks

We emphasize at the outset that concrete is a random composite material at many length scales,[12] from the nanometer scale of the calcium silicate hydrate gel to the micrometer scale of the cement paste to the millimeter and centimeter scale of the aggregate particles. Thus, it is not practical to describe the electrical properties from the material structure by simultaneously considering all these length scales. In this paper, we are concerned with the 10 μm $\rightarrow$ 1000 μm scale that describes a typical mortar.[13,14] Within this framework, mortar can be viewed as a *three-phase composite*[15,16]: matrix cement paste, aggregate sand grains, and interfacial zone cement paste (see Fig. 1), where all three phases can be thought of as uniform continuum materials, characterized by a single conductivity per phase. The thickness of the interfacial zone can vary between 10 and 50 μm.[17] The volume fraction oc-

[a]Permanent address: Schlumberger-Doll Research, Ridgefield, CT 06877-4108; Electronic mail: schwartz@ridgefield.sdr.slb.com

 0021-8979/95/78(10)/5898/11/$6.00

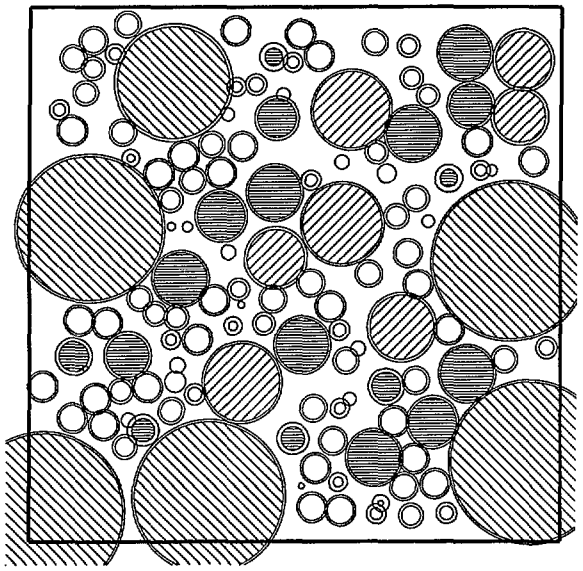

FIG. 1. A slice through the four size random sphere parking model is shown. The total volume fraction of sand is 54% and the distribution of the four aggregate grain sizes is summarized in Table I. The 500 μm diameter grains are shown as open circles, the 1000 μm diameter grains are shaded horizontally, the 1500 μm diameter grains are shaded at 45°, and the 3000 μm diameter grains are shaded at 270°. The thickness of the interfacial zone (unshaded) is 20 μm, a value that guarantees percolation of the interfacial shells (see Fig. 2). The bulk cement paste occupies the interstitial region outside of all the interfacial zones. Note, that there are several instances in which an interfacial shell intersects the plane of the image but the associated sand grain does not. These appear as isolated (rather than concentric) circles.

cupied by the aggregate particles in a mortar is typically 50%→60% with the remaining volume comprised of bulk and interfacial zone cement paste.

Since the interfacial zone can occupy a significant volume fraction, the physical properties of this phase will certainly have an influence on the overall behavior of the composite. This would be true even if this phase were discontinuous. However, recent modelling and mercury injection experimental work showed that, even if the interfacial zone thickness is no more than 10 μm, this phase can still form continuous percolating channels.[14]

For the purposes of electrical conduction, it is assumed that the sand grains in the mortar are simply inert obstacles to the flow of current. The basic model is then defined by three input units:

(1) the structure of the interfacial layer,
(2) the electrical contrast between this layer and the bulk cement paste, and
(3) the concentration and size distribution of the sand grains.

Following previous models we will assume that the sand grains are all spherical and that the interfacial zones are always spherical shells of constant thickness. While the thickness of the interfacial zone, h, may be as large as 50 μm, mercury intrusion measurements and modelling results[14] suggest that $h=20$ μm is a more typical value. Within this zone, both the pore size and the porosity of the cement paste are larger than in the bulk.[17] Accordingly the conductivity

TABLE I. Size distribution for aggregate sand grains in a typical mortar. The second and third columns give, respectively, the volume and numerical fractions of the four size populations.

Grain diameter (μm)	Volume fraction	Numerical fraction
3000	0.354	0.00718
1500	0.232	0.0376
1000	0.224	0.1226
500	0.190	0.8324

and fluid permeability are higher. We assume that the conductivity within the interfacial shell takes a constant value, σ_s, and that the conductivity of the cement paste, σ_p, is also constant. Assuming that the conductivity inside the interfacial shell is constant is an approximation, since actually there is a gradient of porosity and thus conductivity in this region. Since there is no experimentally established value for σ_s/σ_p, we allow this parameter to vary freely in our calculations. Thus, for a given sand concentration, we study the dependence of the composite conductivity on the value of σ_s/σ_p. We also look at the conductivity as a function of sand concentration for several fixed values of σ_s/σ_p.

B. Periodic models

The random arrangement of multi-sized aggregate particles in real mortars plays an important role in determining the effective properties of the composite. However, ordered periodic arrangements of aggregate grains are easier to handle computationally and provide important qualitative insight. The periodic model considered in this paper is a body-centered-cubic (bcc) packing of spherical sand grains. The edge of the unit cube is 500 μm, the sphere diameter is 400 μm, and interfacial zone thickness, h, is 20 μm. The sphere diameter was chosen as being representative of the size distribution used in Ref. 14. Given these parameters, it can easily be shown that the sand volume fraction is 54%, the interfacial zone occupies roughly 1/3 of the matrix, and that the interfacial zones percolate.

C. Disordered models

To study a mortar with a more realistic random sand grain arrangement, we use the model illustrated in Fig. 1, based on the sand grain size distribution given in Table I. The models were generated by a three dimensional hard core parking algorithm.[18] (The sand grains were randomly placed, largest first and smallest last, such that no sand grains overlapped.) The maximum grain concentration studied was $c\approx 0.55$, based on a model with 6500 particles. Models with 5000 ($c=0.42$), 2000 ($c=0.17$), and 1000 ($c=0.09$) particles were also generated to study systems with lower sand concentrations. In Fig. 2 we show the fraction of the matrix occupied by the interfacial zone, as a function of the interfacial zone thickness. Results are shown for the several aggregate concentrations used. As with the periodic model, interfacial shells of thickness 20 μm were added to each grain, so that the interfacial zone comprised about 28% of the total matrix when $c = 0.55$.

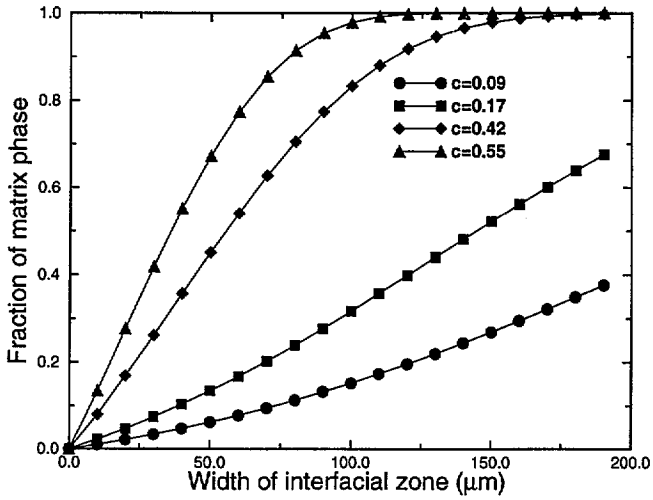

FIG. 2. Given the experimentally determined size distribution (see Ref. 14) of sand grains (assumed spherical), the fraction of the total cement paste volume occupied by the interfacial zone cement paste is shown as a function of the interfacial zone thickness. Results are given for four aggregate concentrations.

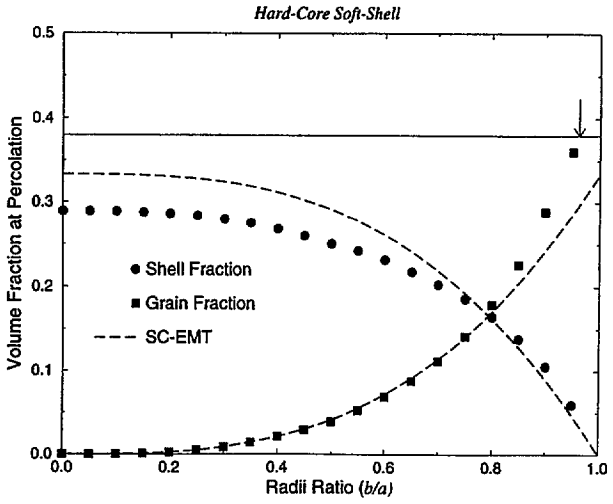

FIG. 4. The percolation properties of interfacial zone in the *mono-sized* random parking model are illustrated by two curves. As functions of the ratio of the sand grain radius, b, to the interfacial zone radius, a, we plot the volume fractions occupied *at the percolation threshold* by (1) the interfacial shell and (2) the aggregate grains. Also shown are the volume fraction corresponding to the limit of dense random parking and the SC-EMT estimates of the shell and aggregate fractions at percolation. The arrow indicates the largest b/a value at which percolating shells can be achieved for dense parking

The connectivity of the interfacial zones was computed using a burning algorithm[14] and is displayed in Fig. 3 as a function of sand volume fraction. The interfacial layers first percolate at a sand concentration of about 36% and form a single spanning cluster at roughly $c \approx 0.51$. The arrow marks the prediction of the self-consistent effective medium theory (SC-EMT) which will be discussed in Sec. III D. To illustrate the interplay between sand volume fraction and interfacial zone thickness, we also studied a simpler disordered model, where the sand grains were all the same size, but the interfacial shell thickness, h, was allowed to vary.[19,20] The controlling variable is then b/a, where b is the sand radius and $a=b+h$. For a given choice of b/a, suppose that we randomly park spherical grains until their concentration, c, is such that the shells form connected channels. The larger the value of b/a (i.e., the thinner the shells), the *greater* the value of c that will be required and the *smaller* the fraction of space that will be occupied by the percolating shells. This behavior is clearly shown in Fig. 4. Shown also are the value of the limiting concentration $c \approx 0.38$ for mono-size random parking,[18] and curves based on the SC-EMT (Sec. III D). Note that there is a threshold value of $b/a \approx 0.9615$ above which it is not possible to form connected percolating shells based on the random parking algorithm.

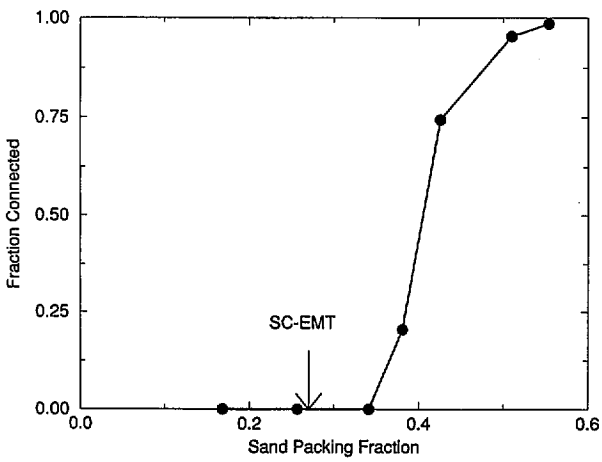

FIG. 3. Percolation curve for the four size random sand grain model with a 20 μm thick interfacial zone. The x-axis is the sand volume fraction, and the y axis is the fraction of the interfacial zone phase that is contained in the percolating cluster.

While the model we pursue in the remainder of this paper is highly simplified, we emphasize that its essential features could be specified in detail if more experimental data on the structure and transport properties of mortars were available. Since the focus of this paper is electrical conduction, it would be particularly valuable to have such measurements made in systems where both the conductivity of the (bulk) cement paste and the porosity and thickness of the interfacial zone were known. In addition, we feel that nuclear magnetic resonance (NMR) studies would be of great value in determining the model's parameters. NMR results would be especially useful if the larger pores in the interfacial zone could be seen in relaxation studies as an independent contribution to the pore size distribution.[21,22] In principle, similar information is available directly from microscopy, but NMR has the advantage of being a non-destructive, non-invasive measurement.

III. COMPUTATIONAL METHODS

A. Periodic model: Finite element calculations

To compute the overall conductivity of this periodic composite, the bcc unit cell, containing two sand grains, was digitized into a 3-D array of pixels, typically 128^3 in size. A

macroscopic electric field was applied in one of the principal cubic directions. Each pixel is then treated as a tri-linear finite element, which results in a set of 128^3 linear equations that are solved with a conjugate gradient algorithm.[23] A resolution of 64^3 was also used, with only very small changes in overall results, so the 128^3 resolution was judged to be adequate to represent both the sand grain, and more importantly, the thin interfacial zone volume. We have also carried out finite difference calculations on identical 3-D grids. Generally, the finite element calculations lead to conductivities that are between 2% and 8% higher than the corresponding finite difference results. Physically, this difference is associated with the fact that the finite element calculations map onto a resistor network with second and third neighbor coupling, while the finite difference calculations map onto a resistor network with nearest neighbor coupling only. A brief comparison of these two methods is presented in the Appendix.

B. Disordered model: Random walk calculations

The conductivity of the random sand grain mortar model was computed quite differently from that of the periodic model. The largest unit cell presently employed in our conjugate gradient-finite element bcc calculations is 128^3. Such calculations typically require 300 megabytes of memory, which scales as the third power of the system length. This is not enough resolution to adequately represent more than a few grains and their associated interfacial zones. To compute the conductivity of statistically representative volumes of disordered systems containing thousands of sand grains requires a different approach.

Here we adopt a random walk algorithm, used extensively in studies of disordered porous media[24–26] and composite materials. For a system in which only one phase has a non-zero conductivity, the algorithm is especially simple. Random walkers are started at various positions in the conductive phase, and allowed to take steps of fixed length, ϵ, in random directions at every time step. The mean-square distance traveled by each walker is computed as a function of the number of time steps. If a projected step would take the walker into the insulating phase, then that step is not allowed, but the clock is still advanced one time step. Eventually, the mean squared distance versus number of time steps is a straight line, whose slope is the diffusion coefficient of the conductive phase. Multiplying by the volume fraction of the conducting phase then gives the overall conductivity of the composite, normalized by the conductivity of the pure conducting phase.[24] More details of the method are available in the Appendix.

When two or more phases are conducting, with different conductivities assigned to each phase, then the algorithm is somewhat more complicated. Within the framework of lattice random walks this problem has been studied by Hong *et al.*[26] In the Appendix we discuss the extension of the methods developed in Ref. 26 to the study of continuum systems. In the present framework, the principle advantage of the random-walk approach is that the aggregate and interfacial structure can be stored as geometrical objects rather than

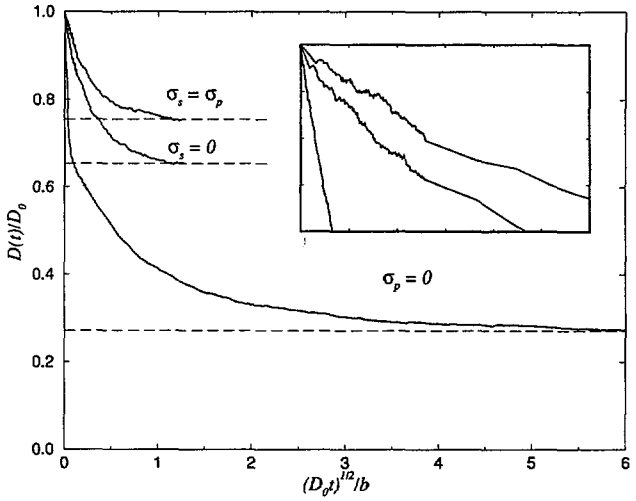

FIG. 5. The effective diffusion coefficient is plotted as a function of time for three systems based on the four size, $c = 0.54$, packing shown in Fig. 1. Results are shown for $\sigma_s/\sigma_p = 1$, $\sigma_s/\sigma_p = 0$ (i.e., insulating interfacial zone), and $\sigma_s/\sigma_p = \infty$ (i.e., insulating bulk paste). The inset highlights the short time behavior of these three curves.

collections of pixels, so that the resolution is essentially that of the step size used. The step size must be small compared to the interfacial zone thickness h, but this can be accomplished *without* any increase in the computational storage required. Of course, run times will increase as the step size decreases, because the walkers must cover several aggregate grain diameters in order to properly estimate the overall conductivity. It should be emphasized that the number of time steps required in these calculations can be very large compared to the corresponding number for calculations of bulk (i.e., single phase) conductivity. Thus, in Fig. 5 we compare the behavior of the effective diffusion coefficient, $D(t)$, for two bulk calculations with the limiting case of purely interfacial conduction. The longer times required in the latter calculation reflect the more tortuous paths connecting the overlapping interfacial shells. At short times the behavior of $D(t)$ is controlled by the surface area to pore volume ratio, S/V_p, of the conducting phase.[27] This ratio is largest for the case in which the interfacial shells alone comprise the conducting channels, as is seen quite clearly in the inset to Fig. 5.

C. Dilute limit

Consider next the limit of dilute sand concentrations. The composite conductivity in this regime contains important information about the conductivity and size of the interfacial zone. This is the case because exact analytical calculations can be made of the influence of a few sand grains (each of which is surrounded by an interfacial shell) placed in a matrix. For the composite to be considered to be in the dilute limit, the volume fraction of spherical inclusions must be small enough so that particles can be treated individually and do not affect each other.

Consider mono-size spherical particles of conductivity

σ_1 and radius b, each surrounded by a concentric shell of thickness h and conductivity σ_2, and all embedded in a matrix of conductivity σ_3. If the volume fraction of sand grains is denoted by c, then the composite conductivity, σ, will satisfy an equation of the form $\sigma/\sigma_3 \equiv 1+mc+O(c^2)$, where[6]

$$m=\frac{\{(\sigma_1-\sigma_2)(2\sigma_2+\sigma_3)+([(b+h)/h])^3(\sigma_1+2\sigma_2)(\sigma_2-\sigma_3)\}}{\{(\sigma_2+2\sigma_3)(\sigma_1+2\sigma_2)+2[b(b+h)]^3(\sigma_1-\sigma_2)(\sigma_2-\sigma_3)\}}. \tag{3.1}$$

To make the connection to our mortar problem, let $\sigma_1=0$, h = the interfacial zone thickness, $\sigma_2=\sigma_s$ (interfacial zone conductivity), and $\sigma_3=\sigma_p$ (bulk cement paste conductivity). For the random mortar model, or indeed for a real mortar, there is a size distribution of sand grain radii $\{b_i\}$, while the value of h is fixed. That implies that the slope m_i for each kind of particle will be a function of b_i, because the parameter $[(b_i+h)/b_i]^3$ will be different for each particle. In a system with N different sand particle sizes, each with volume fraction c_i ($\Sigma_i c_i=c$), we have

$$\frac{\sigma}{\sigma_p}=1+\sum_{i=1}^{N} m_i c_i+O(c^2)\equiv 1+\langle m\rangle c+O(c^2), \tag{3.2}$$

where the terms of order c^2 can be ignored in the dilute limit and play no role in the formulation of effective medium theories. Using the sand particle size distribution given in Table I (second column) we can find the value of $\langle m\rangle$ for the random mortar model averaged over the appropriately weighted four values of b_i.

Figure 6 shows a graph of this average slope $\langle m\rangle$ as a function of σ_s/σ_p. Note in the limit of $\sigma_s/\sigma_p=1$, the slope $\langle m\rangle=-1.5$, which is the known exact result for insulating spherical inclusions of any size distribution.[28,29] The marked point on the graph is at $\sigma_s/\sigma_p\approx 8.26$, which is the point at which the slope $\langle m\rangle=0$. At this value, to linear order in c, adding a few sand grains would *have no effect on the overall conductivity*. Here one has a perfect balance between the negative influence of the insulating sand grains, and the positive effect of the enhanced conductivity in the interfacial shells.

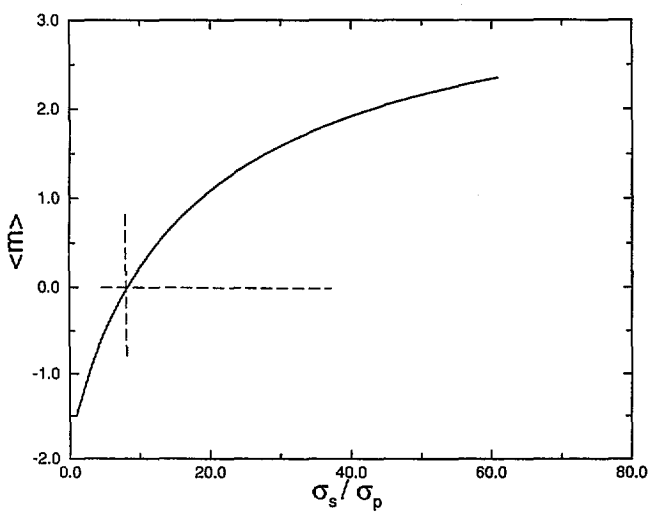

FIG. 6. The exact initial slope of the conductivity, in the limit of dilute sand concentration, is shown as a function of σ_s/σ_p for the sand size distribution (see Table I) of the random model.

D. Effective medium theory

Strictly speaking, the only exact results available for three dimensional composite materials with general properties are variational bounds[30] and the dilute limits presented above. However, effective medium theory (EMT) can often be employed to estimate composite properties at arbitrary volume fractions of the phases.[31,32] We consider only examples of EMT that describe properly the dilute limit, and then build up approximate analytical equations via some sort of averaging assumption. The two examples considered in this paper are the self-consistent (SC-EMT)[31] and the differential (D-EMT)[32] methods.

The SC-EMT has roots going back to Bruggeman[33] and Landauer.[34] Following the presentation of Hashin[31] we begin with an isotropic inhomogeneous system in which the applied electric field has magnitude E_0. In particular we are interested in a three-phase composite with conductivity σ_i and volume fraction c_i in the ith phase. Then the effective conductivity, σ, of the entire composite can be defined by

$$\sigma=\frac{1}{E_0}\sum_i c_i\sigma_i\langle \mathbf{E}(\mathbf{r})\rangle_i \tag{3.3}$$

where σ_i is constant in each phase and $\langle\ldots\rangle_i$ denotes a volume average over V_i, the volume of the ith phase. Also, we have the fundamental theorem[30] that the macroscopic field must satisfy

$$E_0=\sum_i c_i\langle \mathbf{E}(\mathbf{r})\rangle_i. \tag{3.4}$$

Combining these two equations, we can then eliminate the average over the matrix, $i=3$, phase and write the effective conductivity as depending only on averages of electric fields in the non-matrix or inclusion phases:

$$\frac{\sigma}{\sigma_3}=1+c_1\left(\frac{\sigma_1}{\sigma_3}-1\right)\frac{\langle \mathbf{E}(\mathbf{r})\rangle_1}{E_0}+c_2\left(\frac{\sigma_2}{\sigma_3}-1\right)\frac{\langle \mathbf{E}(\mathbf{r})\rangle_2}{E_0} \tag{3.5}$$

where phase 1 is the sand grain and phase 2 is the shell. The above equation is exact. However, at arbitrary volume fractions, the above field averages cannot be evaluated analytically. (In principle, the finite element method discussed above could give these field averages numerically.) The SC-

EMT is derived by making the assumption that the field averages can be approximated by inserting the values obtained from a modified dilute problem, in which the inclusions are embedded, not in phase 3, but in a matrix having the effective conductivity σ. This transforms Eq. (3.5) into an equation for σ, which can then be solved.

The four sizes of sand grains used in our model are simply treated as different phases. The shell volume fractions are estimated by assuming that the shells do not overlap. Numerical checks have shown that this is accurate to a few percent in even the concentrated sand case. This means that even though the shells percolate, the overlap volume is only a few percent of the total shell volume. For a single size sand grain embedded in a matrix of conductivity σ, the field averages for the sand grain and the shell are given by:

$$\langle \mathbf{E}(\mathbf{r})\rangle_1 = \frac{E_0}{H}; \quad \langle \mathbf{E}(\mathbf{r})\rangle_2 = \left(\frac{\sigma_1+2\sigma_2}{3\sigma_2}\right)\frac{E_0}{H} \tag{3.6}$$

where

$$H = \frac{1}{9\sigma_2\sigma}\left((\sigma_2+2\sigma)(\sigma_1+2\sigma_2) + \frac{2b^3}{(b+h)^3}(\sigma_1-\sigma_2)(\sigma_2-\sigma)\right), \tag{3.7}$$

and the labels 1 and 2 denote the sand grain and shell, respectively. Combining these with Eq. (3.5), and averaging over the different size sand grains, gives the final result. For the mortar problem, we take $\sigma_1=0$, $\sigma_2=\sigma_s$, and $\sigma_3=\sigma_p$. The structure of the SC-EMT leads to a natural division of the possible behavior of the total conductivity for different values of σ_s/σ_p. When the value of σ_s/σ_p is such that the dilute limit slope, $\langle m\rangle$, is zero, then the SC-EMT continues to give the matrix conductivity for *any* volume fraction of sand [i.e., $\sigma=\sigma_p$ is a *fixed* point of the theory when $\langle m\rangle=0$ in Eq. (3.1)]. When σ_s/σ_p is greater than this value, $\sigma\geq\sigma_p$, while for lower σ_s/σ_p values, $\sigma\leq\sigma_p$, for all sand volume fractions.

In the D-EMT the dilute limit (3.1) is used in a different way to generate an approximate equation that can be solved for the effective conductivity.[32,33] Suppose that a volume fraction, c', of sand has been placed in the matrix. This system is treated as a homogeneous composite with conductivity σ' and matrix volume fraction, $\phi'\equiv 1-c'$. We then suppose that a differential volume element, dV, of the composite material is removed and replaced by an equivalent volume of sand. The new conductivity, $\sigma'+d\sigma'$, is assumed to be given by the dilute limit

$$\sigma'+d\sigma' = \sigma'+m(\sigma')\frac{dV}{V} \tag{3.8}$$

where V is the total volume and $m(\sigma')$ is given by (3.1) with $\sigma_3\to\sigma'$. When the volume element dV was removed, only a fraction, $\phi'=1-c'$, of it was matrix material so that the actual change in the matrix volume fraction, $d\phi'$, is given by

$$d\phi' = -\phi'\frac{dV}{V}. \tag{3.9}$$

Equation (3.8) then reduces to $d\phi'/\phi' = -d\sigma'/m(\sigma')$, which can be integrated to yield

$$-\int_{\sigma_3}^{\sigma}\frac{d\sigma'}{m(\sigma')\sigma'} = \int_1^{\phi}\frac{d\phi'}{\phi'} = \ln(\phi) = \ln(1-c), \tag{3.10}$$

where $c=1-\phi$ is the material's final sand concentration. If more than one size sand grain is used, then the function $m(\sigma)$ must be viewed as an average over the size distribution of sand grains. In that case, the integral can be done numerically for chosen values of σ, with the sand volume fraction $c=1-\phi$ then treated as being a function of σ. For a single size sand grain, the final equation can be found analytically, and is given by:

$$c = 1-\left(\frac{\sigma}{\sigma_3}\right)^{g/e}\left(\frac{k\sigma+e}{k\sigma_3+e}\right)^{(g/e-f/k)}, \tag{3.11}$$

where

$$g = \sigma_2(\sigma_1+2\sigma_2)+2\left(\frac{b}{b+h}\right)^3\sigma_2(\sigma_1-\sigma_2), \tag{3.12a}$$

$$f = 2(\sigma_1+2\sigma_2)-2\left(\frac{b}{b+h}\right)^3(\sigma_1-\sigma_2), \tag{3.12b}$$

$$e = 3\left[2\sigma_2(\sigma_1-\sigma_2)+\left(\frac{b+h}{b}\right)^3\sigma_2(\sigma_1+2\sigma_2)\right], \tag{3.12c}$$

$$k = 3\left[(\sigma_1-\sigma_2)+\left(\frac{b+h}{b}\right)^3(\sigma_1+2\sigma_2)\right]. \tag{3.12d}$$

As for the SC-EMT, the D-EMT gives a fixed point when the slope $m(\sigma)$, equals zero. This is easy to see in the present (D-EMT) case, because the first step of adding inclusions to the original matrix will produce a transformed matrix with the *same* conductivity as the original bulk paste. Successive iterations, again, lead to no change in σ.

Both the SC-EMT and the D-EMT are correct in the dilute limit. Another figure of merit for an EMT is how well any percolation threshold is predicted.[35] In particular, the volume fraction of shells at which the shell phase first percolates is of interest, because of the possibility of having a large conductivity in the shells. In the EMT equations, the predicted percolation threshold may be found by allowing the matrix conductivity to go to zero, and determine at what value of the shell volume does the effective conductivity become non-zero. If the matrix conductivity is zero, the only way for the composite conductivity to be non-zero is if the interfacial zone regions percolate. The D-EMT gives a percolation threshold only at a sand volume of 1, which is clearly wrong (see Fig. 3). The SC-EMT for mono-size spherical sand grains of radius, b, and shell thickness, h, predicts a critical threshold for the shell phase at a shell volume fraction of $(1/3)[1-(b^3/(b+h)^3]$, or, alternatively, for a sand volume fraction of $b^3/[3(b+h)^3]$. Figure 3 shows both these predictions plotted versus b/a $(a=b+h)$ along with the numerically determined percolation thresholds. There is indeed reasonable agreement. The region of interest is where $b/a\geq 0.7$, since that is the typical lower limit for $b/(b+h)$ because the smallest b found in mortar is of the order of 50 μm, and h is usually of the order 20 μm.

In this region, the SC-EMT prediction is qualitatively correct for the shell volume fraction, but does not give the correct curvature. The prediction for the sand volume fraction is increasingly off as h goes to zero, since the SC-EMT does not correctly predict the volume fraction at the random parking limit.[18] Still, this shows that since the dilute limit is correctly predicted, and the percolation threshold is reasonably well predicted, the SC-EMT might be expected to do fairly well in between these two limits. Because of this difference between the two methods, we expect that for $\sigma_s/\sigma_p \gg 1$, the SC-EMT will work better than the D-EMT. This is because the percolation threshold, at which the effective composite conductivity will eventually diverge, is not properly accounted for in the differential method.

If we consider the SC-EMT for the four sand grain radii model, we can numerically determine what is the predicted sand volume fraction at which the interfacial zones percolate. The SC-EMT prediction is $c=0.27$, which is reasonably near the result of Fig. 3, $c \approx 0.36$.

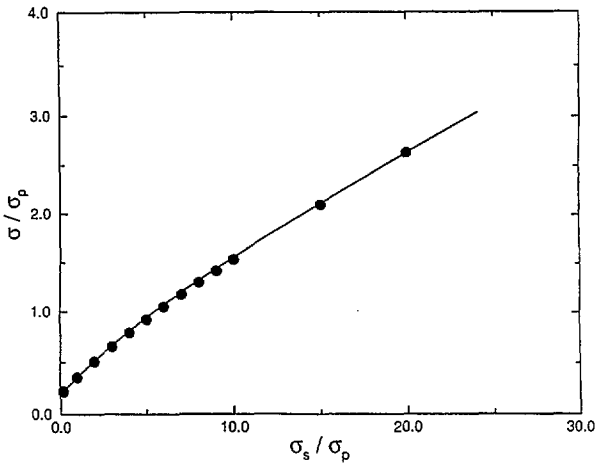

FIG. 7. Composite conductivity for the bcc model is plotted vs the interfacial zone conductivity (both are normalized by the bulk paste conductivity). The solid dots are the numerical data, the solid line is the Padé approximant based on the parameters values: $F=2.82$, $\Lambda=88.8$ μm, $\lambda=560.0$ μm, and $f=20.0$ μm.

E. Padé approximants

Padé approximants can be employed[11,36] to describe the conductivity of porous sandstone rocks where the sand grains have a thin clay coating that has a higher conductivity than the electrolytic pore fluid. This is a situation analogous to the mortar and concrete conductivity problem being studied here. The Padé approximant in this case is a ratio of a quadratic polynomial to a linear polynomial,

$$\frac{\sigma}{\sigma_p}=\frac{b+cx+dx^2}{1+ax} \tag{3.13}$$

where $x=\sigma_s/\sigma_p$. The parameters a, b, c, and d are given by combinations of four well-defined parameters F, Λ, f, and λ which are defined in terms of two limits of the effective conductivity.[11]

The first limit, in which the interfacial zone is only slightly more (or slightly less) conductive than the bulk cement paste matrix, $\sigma_s/\sigma_p \to 1$, is given exactly by perturbation theory as[11]

$$\frac{\sigma}{\sigma_p}=\frac{1}{F}\left(1+\frac{2h(\sigma_s/\sigma_p-1)}{\Lambda}\right) \tag{3.14}$$

where $1/F$ is the ratio of the conductivity of the mortar to the conductivity of the bulk paste when $\sigma_s/\sigma_p = 1$, and Λ is a pore scale length parameter calculated in terms of the electric fields associated with the $\sigma_s=\sigma_p$ problem.[11] When $\sigma_s/\sigma_p=1$, $\sigma/\sigma_p=1/F$, and when σ_s/σ_p is close to 1, Eq. (3.13) is linear in σ_s/σ_p with a slope given by the ratio $2h/(F\Lambda)$.[11]

The second limit is when the conductivity of the interfacial zone is much larger than that of the bulk cement paste, $\sigma_s/\sigma_p \gg 1$. Assuming that the interfacial zones percolate, the composite conductivity in this limit is given by perturbation theory as[11]

$$\frac{\sigma}{\sigma_p}=\frac{1}{f}[h(\sigma_s/\sigma_p-1)+\lambda/2] \tag{3.15}$$

where f and λ are additional length parameters defined in terms of the solutions of the $\sigma_p=0$ and $\sigma_s=1$ problem.[11] Fitting Eq. (3.13) to Eqs. (3.14) and (3.15) gives the four unknown coefficients a, b, c, and d.

IV. CONDUCTIVITY RESULTS

A. Periodic model

We first present the results for the bcc periodic model described in Sec. II B. Figure 7 shows the normalized conductivity of the composite; σ/σ_p, as a function of σ_s/σ_p. The interfacial zone cement paste percolates in this model, and so plays a strong role in the overall conductivity, as can be seen from the graph. Three points are worthy of note. First, the conductivity at $\sigma_s/\sigma_p = 1$ is that which would be obtained if the interfacial zone cement paste had the same porosity and therefore the same conductivity as the bulk cement paste. The presence of the insulating sand grains in this case reduces the overall normalized conductivity from 1 to 0.35. This is consistent with a 3/2 power law found in suspensions of spheres. In this case, $(0.46)^{3/2} = 0.31$.[28,29,37] Second, as we noted in connection with Fig. 6, the composite conductivity can be viewed as the result of a competition between the insulating sand grains and the interfacial shells. Figure 7 shows that when $\sigma_s/\sigma_p \approx 6$, the composite conductivity first achieves a value equal to the matrix conductivity, so for this microstructure, this value of σ_s/σ_p causes the greater interfacial zone conductivity to cancel out the effect of the insulating sand grains. Third, the Padé approximant provides an excellent fit to the computed data points in Fig. 7, so that this analytical curve could be used to accurately *predict* the composite conductivity at other values of σ_s/σ_p that were not numerically computed. (Here the four parameters F, Λ, f, and λ were computed directly from the finite element solutions for two limiting cases, $\sigma_s=\sigma_p$ and $\sigma_p=0$; their values are $F=2.82$, $\Lambda=88.8$ micrometers, $\lambda=560.0$ micrometers, and $f=20$ micrometers.)

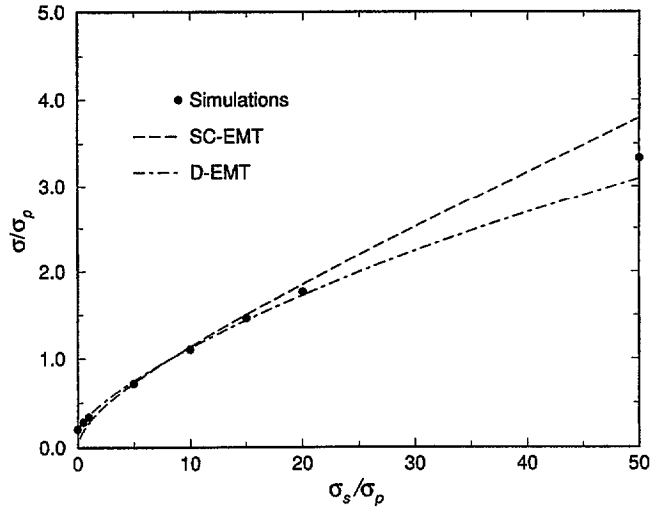

FIG. 8. Composite conductivity for the random model is plotted vs the interfacial zone conductivity (both are normalized by the bulk paste conductivity). The solid dots are the random walk data; also shown are the SC and D-EMT results.

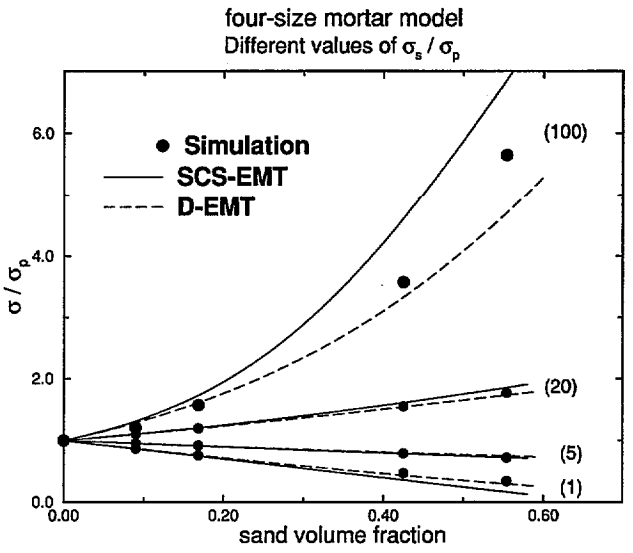

FIG. 9. Composite conductivities (calculated by random walk simulations) for the random model are shown as a function of sand concentration for four values of the interfacial zone conductivity. The relevant values of σ_s/σ_p are indicated in parenthesis on the right. Also shown are the corresponding predictions of SC and D-EMT (normalization is as in Figs. 7 and 8).

B. Disordered models

In Fig. 8 we present the random walk simulation results for the disordered four grain size model together with the predictions of the SC-EMT and the D-EMT. We note that, as in Fig. 7, the overall shape of the curves is concave down. The simulation data could at most form a straight line. This would be the case if the two conducting phases, interfacial zone and bulk cement paste, were exactly in parallel. Then the overall conductivity would be given by a simple linear combination of the two phase conductivities, and as σ_s increased, the overall conductivity would increase linearly. Since the microstructure is such that these two cement paste phases are not in parallel, the curve must be sub-linear, or concave down. As $\sigma_s/\sigma_p \to \infty$ the curve will eventually become straight as predicted by Eq. (3.15).

The data in Fig. 8 indicate that to achieve an overall conductivity that is equal to the bulk cement paste conductivity, the value of σ_s/σ_p must be equal to approximately 8. This is higher than the corresponding value obtained in the bcc model, due to the greater tortuosity and smaller volume fraction of the interfacial zone in the present case. Increasing σ_s/σ_p has therefore a somewhat smaller effect on the overall conductivity. At $\sigma_s/\sigma_p = 20$, $\sigma/\sigma_p \approx 1.8$, which is significantly less than the corresponding bcc value for the same reasons. We have attempted to fit the simulation data shown on Fig. 8 with a Padé approximant (not shown) similar to that in Fig. 7. The fit is less satisfactory than in the bcc case but is no worse than that offered by the two EMT curves. Again, this is an indication of the greater complexity of the random four grain size model.

Consider next the behavior of the conductivity as a function of the sand volume fraction (Fig. 9). In Fig. 8 we saw that, at a sand volume fraction of 55%, a value of $\sigma_s/\sigma_p \approx 8$ was required to make the composite conductivity equal to the bulk cement paste conductivity. This is remarkably close to the dilute limit result $\sigma_s/\sigma_p \approx 8.26$ found in Fig. 6 and is in agreement with the EMT predictions discussed earlier. Viewing σ/σ_p as a function of sand concentration, these results imply that for $\sigma_s/\sigma_p \leqslant 8.26$, σ/σ_p must start out with negative slope and remain less than unity. By contrast, for $\sigma_s/\sigma_p \geqslant 8.26$, the curve starts out with positive slope and is always greater than unity. Because the dilute limit defines the essential features of the overall curve, the SC-EMT and D-EMT should correctly predict the essential structure of the composite conductivity. This is clearly evident in Fig. 9.

Figure 9 shows computed conductivity data for the random mortar model as a function of sand volume fraction, for $\sigma_s/\sigma_p = 100$, 20, 5, and 1. The sand size distribution was preserved at every volume fraction. The curves for $\sigma_s/\sigma_p = 100$ and 20 are concave up, with the $\sigma_s/\sigma_p = 100$ results showing clear evidence of the interfacial zone percolation threshold. The $\sigma_s/\sigma_p = 5$ and 1 curves have negative initial slopes, and remain below one, as expected. The $\sigma_s/\sigma_p = 1$ curve roughly follows a 3/2 power law in the total cement paste volume fraction, as would be expected since there is no difference between interfacial zone and bulk cement paste in this case.

Two features of the SC-EMT and D-EMT predictions are worth noting. First, for $\sigma_s/\sigma_p \geqslant 5$, the SC-EMT is always above the D-EMT prediction, while for $\sigma_s/\sigma_p \leqslant 5$, this situation is reversed. For very large values of the interfacial shell zone conductivity, the SC-EMT is clearly much above the data while the D-EMT is clearly well below the data. This is due to the fact that the SC-EMT predicts the interfacial zone percolation point at a lower volume fraction than is realistic, while the D-EMT predicts too high of a sand volume fraction at percolation. Second, there are several ways to take the limit of EMT when $\sigma_s \to \sigma_p$. One can take $h \to 0$, or take $\sigma_s \to \sigma_p$; these limits give different results. For example, the

D-EMT gives the well-known 1.5 power law when $h \to 0$, but does not when $\sigma_s \to \sigma_p$ with $h \neq 0$. Since the data clearly follow this power law in this limit, we employ the $h \to 0$ limit for both the SC and D-EMT to describe the $\sigma_s = \sigma_p$ system.

V. FLUID FLOW

The present model for interfacial transport can, approximately, be extended to include fluid permeability. The correct way to calculate the permeability of a mortar would be to solve the Navier-Stokes equations for the random pore space,[38,39] which would include bulk cement paste pores as well as interfacial cement paste pores. However, since we are considering mortar at *intermediate* length scales in this paper, we can use Darcy's law,[38] with the appropriate permeabilities, for the three component composite: sand (K_a), interfacial zone cement paste (K_s), and bulk cement paste (K_p). The relevant equation for such a description of systems with spatially varying permeability is[38,40]

$$\mathbf{V}(\mathbf{r}) = -\frac{K(\mathbf{r})\nabla P(\mathbf{r})}{\eta} \tag{5.1}$$

where $\mathbf{V}(\mathbf{r})$ is the macroscopic fluid velocity, $K(\mathbf{r})$ is the permeability, $P(\mathbf{r})$ is the pressure at a position $\mathbf{r}$, and η is the fluid viscosity. If we identify $\mathbf{V}(\mathbf{r})$ with $\mathbf{j}(\mathbf{r})$, the electrical current density, $K(\mathbf{r})/\eta$ with the electrical conductivity, and $P(\mathbf{r})$ with the electrostatic potential, then this equation reduces to the equation for steady-state electrical current flow. The boundary conditions for the two problems are also identical, so that all the results we have obtained for electrical conductivity can be re-interpreted for fluid permeability, albeit approximately.

Within this framework, an essential step is to estimate the value of K_s/K_p, the parameter analogous to σ_s/σ_p. Here we propose to use the Katz-Thompson equation,[41] which predicts the permeability of a porous medium in terms of its electrical conductivity and a critical pore radius characteristic of the largest connected pores in the material as defined by a mercury intrusion experiment. The equation derived in Ref. 41 has been shown to work reasonably well on cement-based materials.[42,43] Neglecting constants of proportionality, the relevant equation is $k \sim d^2/F$, where F is the formation factor defined in Eq. (3.14) and d is the critical pore diameter. If we assume that the value of d for interfacial zone cement paste is about 10 times larger than that for the bulk cement paste, in rough agreement with the available mercury intrusion data,[14] and take the interfacial zone conductivity to be about 10 times larger than that of the bulk cement paste, as suggested by recent experiments on synthetic interfaces,[44] the resulting estimate is $K_s/K_p \approx 1000$. The largest value of σ_s/σ_p computed in Fig. 8 was only 100, but we can use either the fitted Padé approximant or the two effective medium theories to obtain the result $K/K_p \approx 35$ for the effective permeability ratio. Data in Ref. 43 indicate that the permeabilities of mortars with about 50% sand concentration are between 20 and 60 times higher than that of the bulk cement paste, in agreement with the above estimate.

VI. CONCLUSIONS

We have developed a model for interfacial transport in a class of three phase composite materials that provides a reasonable starting point for the description of mortar and concrete. Assuming that the interfacial zone has a well-defined thickness and conductivity, we have shown how its presence influences the overall conductivity of the composite material. Although the aggregate size distribution used in our numerical calculations was typical of a mortar the same general behavior is expected in concrete. Since the interfacial zone cement paste occupies a significant fraction of the total cement paste phase (up to one quarter or one third) and often forms a percolating channel, the higher conductivity of this phase will cause the overall conductivity of the mortar to be significantly higher than the value that would be obtained from a simple two-phase (bulk cement paste plus aggregate) composite model. The essential parameters of our model are the ratio σ_s/σ_p, the thickness, h of the interfacial zone, and the aggregate concentration, c. For small values of c we have shown that the overall conductivity can be predicted analytically, for any given sand size distribution. For larger values of c, numerical calculations on three dimensional models are required and we have shown that random walk techniques can perform this task accurately.

ACKNOWLEDGMENTS

We are grateful to Daniel Hong for useful conversations concerning the random walk algorithm in composites with two conducting phases. This work has been supported in part by the National Science Foundation, via the Science and Technology Center for Advanced Cement-Based Materials. LMS thanks NIST for partial support of his sabbatical leave from Schlumberger-Doll Research.

APPENDIX: TWO PHASE RANDOM WALK CALCULATIONS

In all random walk calculations, our objective is to estimate the mean squared displacement, $\langle r^2(t) \rangle$, of a collection of walkers as a function of time, t. At *long* times this quantity varies as $\langle r^2(t) \rangle \sim Dt$, where D is the effective diffusion coefficient of the pore space only. D is related to the measured diffusion coefficient of the entire sample, D_T, which is referred to the entire cross-sectional area of the sample, by a factor of porosity ($D_T = \phi D$). The conductivity is then given by

$$\frac{\sigma}{\sigma_p} = \phi \frac{D}{D_p} \tag{A1}$$

where σ_p and D_p are the pure phase coefficients of phase p.

Consider a two phase medium in which the conductivity in one phase is unity and in the other phase is $h \leqslant 1$. The simplest random walk is sometimes referred to as a *blind* walk. Within a given phase, the walker takes steps of length ϵ, but the time increment associated each step is inversely proportional to the conductivity. Operationally, in the high conductivity phase the walker takes steps of length ϵ and the clock advances by a unit increment, τ. [If the proposed step would take the walker into an insulating region (e.g., a sand

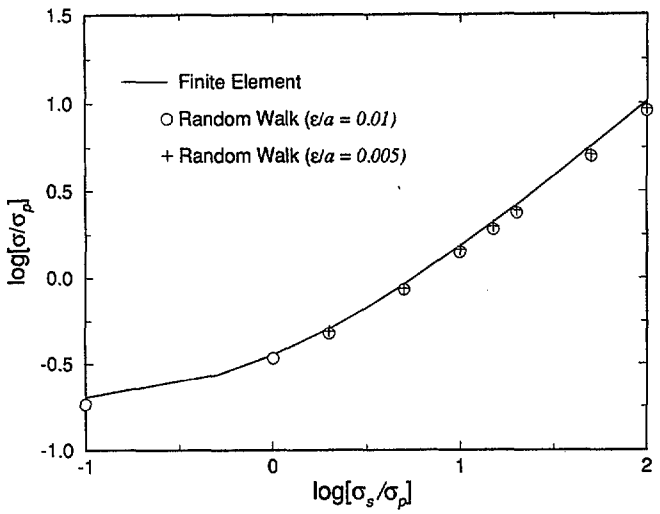

FIG. 10. The effective conductivity is shown for the bcc lattice of spherical grains with overlapping shells. We compare finite element and blind random walk calculations and note that better accuracy is achieved as the random walk step size is reduced.

grain) then the walker is returned to the attempt position but the clock is advanced by τ.] In the low conductivity phase the step length is again ϵ but the walker accepts each proposed step only with probability h, thus spending a certain fraction of the time simply standing still. If walker steps from the high to the low conducting phase (or *vice versa*) the probability for accepting the step is $2h/(1+h)$, as if the corresponding bond was a *series* connection between high and low conductivity bonds. This approach is straightforward although computationally rather inefficient because the walkers spend a certain amount of their time at rest. In Fig. 10 we compare the results of blind random walk calculations with finite element calculations for the bcc lattice described in Sec. III A. Generally the agreement is quite good, although the differences between the two techniques can be as large as 10%.

In a more efficient implementation of the random walk method the walkers are referred to as being *myopic*. The rules in the high conductivity phase do not change. Within the low conductivity phase the walker *always* accepts each proposed step, but the clock is advanced by an amount $1/h$. To this point it does not matter whether we are working on a lattice or in a continuum representation. The distinction between lattice and continuum systems arises only when we consider steps that take the walker from one phase to the other. Here we find that the following rules lead to quite reasonable results:

(1) if the proposed step takes the walker from the high to the low conducting phase the step is accepted with probability h and the clock is advanced by an amount $(1+h)/(2h)$ if the step is accepted and by a unit amount if the step is rejected;
(2) if the proposed step takes the walker from the low to the high conducting phase the step is always accepted and the clock is again advanced by $(1+h)/(2h)$.

With these rules we have consistently obtained results that are in general agreement with blind walker calculations. In the case of the bcc lattice, a comparison of finite element, finite difference, blind walker, and myopic walker calculations is summarized in Table II.

TABLE II. Comparison of finite element, finite difference, and random walk calculations for the bcc lattice described in Sec. II B. The finite element and finite difference calculations were executed on grids of the same size. The blind and myopic walker calculations were done with step size $\epsilon=0.01a$ where a is the length of the unit cell. Some additional calculations (shown in parenthesis) were done with $\epsilon=0.005a$.

Conductivity ratio	Finite element	Finite difference	Blind walkers	Myopic walkers
1	0.355	0.349	0.340	0.350
2	0.508	0.495	0.476 (0.491)	0.486
5	0.921	0.885	0.855 (0.868)	0.866
10	1.53	1.46	1.41 (1.46)	1.42
20	2.63	2.49	2.38 (2.46)	2.45
50	5.60	5.22	5.02 (5.14)	5.13
100	10.25	9.48	9.06 (9.30)	9.40

[1] E. J. Garboczi, Cem. Conc. Res. **20**, 591 (1990).
[2] A. Atkinson and A. K. Nickerson, J. Mater. Sci. **19**, 3068 (1984).
[3] H. F. W. Taylor, *Cement Chemistry* (Academic, San Diego, 1990).
[4] E. J. Garboczi and D. P. Bentz, J. Mater. Sci. **27**, 2083 (1992).
[5] R. T. Coverdale, B. J. Christensen, T. O. Mason, H. M. Jennings, D. P. Bentz, and E. J. Garboczi, J. Mater. Sci. **30**, 712 (1995).
[6] E. J. Garboczi, L. M. Schwartz, and D. P. Bentz, J. Adv. Cem. Based Mater. **2**, 169 (1995).
[7] B. J. Christensen, T. O. Mason, H. M. Jennings, D. P. Bentz, and E. J. Garboczi, MRS Soc. Symp. Proc. **245**, 259 (1992).
[8] C. C. Liang, J. Electrochem. Soc. **120**, 1289 (1973).
[9] J. Maier, Phys. Status Solidi B **123**, K89 (1984).
[10] A. Bunde, W. Dieterich, and E. Roman, Phys. Rev. Lett. **55**, 5 (1985); H. E. Roman, A. Bunde, and W. Dieterich, Phys. Rev. B **34**, 3439 (1986).
[11] D. L. Johnson, T. J. Plona, and H. Kojima, *Physics and Chemistry of Porous Media II* (Ridgefield, 1986); *AIP Conference Proceedings No. 154*, edited by J. Banavar, J. Koplik, and K. W. Winkler (AIP, New York, 1986); L. M. Schwartz, P. N. Sen, and D. L. Johnson, Phys. Rev. B **40**, 2450 (1989).
[12] E. J. Garboczi, Mater. Structures **26**, 191 (1993).
[13] S. Mindess and J. F. Young, *Concrete* (Prentice-Hall, Englewood Cliffs, NJ, 1981).
[14] D. N. Winslow, M. Cohen, D. P. Bentz, K. A. Snyder, and E. J. Garboczi, Cem. Conc. Res. **24**, 25 (1994).
[15] A. Goldman and A. Bentur, Cem. Conc. Res. **23**, 962 (1993).
[16] A. U. Nilsen and P. J. M. Monteiro, Cem. Conc. Res. **23**, 147 (1993).
[17] K. L. Scrivener, American Ceramic Society, Westerville, OH, 1989.
[18] D. W. Cooper, Phys. Rev. A **38**, 522 (1988).
[19] G. E. Pike and C. H. Seager, Phys. Rev. B **10**, 1421 (1974).
[20] A. L. Bug, S. A. Safran, G. S. Grest, and I. Webman, Phys. Rev. Lett. **55**, 1896 (1985).
[21] W. P. Halperin, J.-Y. Jehng, and Y.-Q. Song, Magn. Res. Imag. **12**, 169 (1994).
[22] S. Bhattacharja, M. Moukwa, F. D'Orazio, J.-Y. Jehng, and W. P. Halperin, J. Adv. Cem. Based Mater. **1**, 67 (1993).
[23] J. F. Douglas and E. J. Garboczi, Adv. Chem. Phys. **91**, 85 (1995).
[24] L. M. Schwartz and J. R. Banavar, Phys. Rev. B **39**, 11965 (1989).
[25] I. C. Kim and S. Torquato, Phys. Rev. A **43**, 3198 (1991).
[26] D. C. Hong, H. E. Stanley, A. Conoglio, and A. Bunde, Phys. Rev. B **33**, 4564 (1986).
[27] P. P. Mitra, P. N. Sen, L. M. Schwartz, and P. Le Doussal, Phys. Rev. Lett. **68**, 3555 (1992); P. P. Mitra, P. N. Sen, and L. M. Schwartz, Phys. Rev. B **47**, 8565 (1993).
[28] R. E. De La Rue and C. W. Tobias, J. Electrochem. Soc. **106**, 827 (1959).
[29] P. N. Sen, C. Scala, and M. H. Cohen, Geophys. **46**, 781 (1981).
[30] S. Torquato, Appl. Mech. Rev. **44**, 37 (1991).

[31] Z. Hashin, J. Composite Mater. **2**, 284 (1968).
[32] R. McLaughlin, Int. J. Eng. Sci. **15**, 237 (1977).
[33] D. A. G. Bruggeman, Annalen der Physik **24**, 636 (1935).
[34] R. Landauer, Electrical Transport and Optical Properties of Inhomogeneous Media, AIP Conf. Proc., 1978, p. 2.
[35] W. Xia and M. F. Thorpe, Phys. Rev. A **38**, 2650 (1988).
[36] C. M. Bender and S. A. Orszag, *Advanced Mathematical Methods for Scientists and Engineers* (McGraw-Hill, New York, 1978).
[37] P. Z. Wong, Phys. Today **41**, 24 (1988).
[38] F. A. L. Dullien, *Porous Media: Fluid Transport and Pore Structure*, 2nd ed. (Academic, New York, 1992).
[39] L. M. Schwartz, N. Martys, D. P. Bentz, E. J. Garboczi, and S. Torquato, Phys. Rev. E **48**, 4584 (1993).
[40] A. E. Scheidegger, *The Physics of Flow Through Porous Media*, 3rd ed. (University of Toronto Press, Toronto, 1974), Section 4.3.
[41] A. J. Katz and A. H. Thompson, Phys. Rev. B **34**, 8179 (1986); J. Geophysics Res. **92**, 599 (1987).
[42] B. J. Christensen, R. T. Coverdale, R. A. Olson, S. J. Ford, E. J. Garboczi, H. M. Jennings, and T. O. Mason, J. Amer. Ceram. Soc. **77**, 2789 (1994).
[43] P. Halamickova, R. J. Detwiler, D. P. Bentz, and E. J. Garboczi, Cem. Conc. Res. **25**, 790 (1995).
[44] X. Ping, J. J. Beaudoin, and R. Brousseau, Cem. Con. Res. **21**, 515 (1991).